Correspondence to:
O. Huhn,
ohuhn@uni-bremen.de

Submarine Meltwater From Nioghalvfjerdsbræ (79 North Glacier), Northeast Greenland

Oliver Huhn[1] , Monika Rhein[1,2] , Torsten Kanzow[3] , Janin Schaffer[3] , and Jürgen Sültenfuß[1]

[1]IUP - Institute of Environmental Physics, University of Bremen, Bremen, Germany, [2]MARUM – Center for Marine Environmental Sciences, University of Bremen, Bremen, Germany, [3]AWI - Helmholtz Centre for Polar and Marine Research, Bremerhaven, Germany

Abstract The Greenland Ice Sheet (GrIS) faces accelerated melting under a warming climate. This also affects the largest marine-terminating outlet glacier of the Northeast Greenland Ice Stream (NEGIS), the Nioghalvfjerdsbræ (79 North Glacier, 79NG). In the cavity below its floating ice tongue, the heat of inflowing warm and saline Atlantic Water melts the ice at the base, and colder and fresher outflow is exported toward the shelf break and presumably south with the East Greenland Current (EGC). However, freshwater from submarine melting is hardly distinguishable from other freshwater sources by salinity alone. To identify and to quantify the distribution of submarine meltwater on the Northeast Greenland Shelf, we use helium (He) and neon (Ne) observations obtained directly at the calving front of the 79NG, on the Northeast Greenland Shelf, and in Fram Strait during an expedition aboard R/V POLARSTERN in summer 2016. These tracers uniquely identify submarine meltwater (SMW) and allow quantifying its fraction. SMW is present on the shelf but dilutes from 1.8% at the 79NG calving front to nonsignificant in Fram Strait. The SMW formation rate of the 79NG was estimated to be 14.5 ± 2.3 Gt per year. A surplus of Ne compared to He in the upper 100 dbar observed on most of the shelf region is attributed to noble gas fractionation during sea ice formation. Combining the Ne excess with the ventilation time on the shelf of 1.5 years yields a mean sea ice formation rate of 4 m per year.

Plain Language Summary The Greenland Ice Sheet is melting faster due to global warming. The involved processes are surface melting, iceberg calving, and submarine melting through the contact of the glaciers with warm ocean water. The Nioghalvfjerdsbræ ("79NG") is the largest marine-terminating glacier in northeast Greenland. It has a floating ice tongue. Inside the cavity, heat from warm and salty water melts the ice at the base, and colder and fresher water is exported. However, freshwater from submarine melting is hard to distinguish from other freshwater sources by salinity alone. To identify and to quantify the distribution of submarine meltwater (SMW) on the Northeast Greenland Shelf, we use oceanic helium (He) and neon (Ne) observations. We obtained them directly at the front of the 79NG, on the Northeast Greenland Shelf, and in Fram Strait during a Polarstern expedition in 2016. These light and low soluble noble gases provide a unique tool to identify SMW and to quantify its fractions. We calculate a SMW formation rate of 14.5 ± 2.3 Gt per year of the 79NG. SMW fractions are present on the shelf, but dilute from 1.8% at the 79NG front to nonsignificant in Fram Strait.

1. Introduction

The Greenland Ice Sheet (GrIS) faces accelerated melting under a warming climate, and the GrIS mass loss contributed about 25% to the global sea-level rise in the time period 2006–2015 (Oppenheimer et al., 2019). The involved processes are surface melting, iceberg calving, and submarine melting through the contact of warm water with marine-terminating glaciers and floating ice tongues. N. Wilson et al. (2017) showed that the latter mechanism is the major contributor for mass loss of the three largest floating ice tongues in northern Greenland. The meltwater from the GrIS is not only contributing to global sea-level rise, but could affect the regional circulation by changing the seawater density structure (e.g., Grivault et al., 2017). When transferred into the basin interior of the Labrador and Irminger seas, this additional freshwater might have consequences for the water mass transformation of Atlantic Meridional Overturning Circulation components (Böning et al., 2016). The analysis of noble gas data revealed that the presence of submarine meltwater
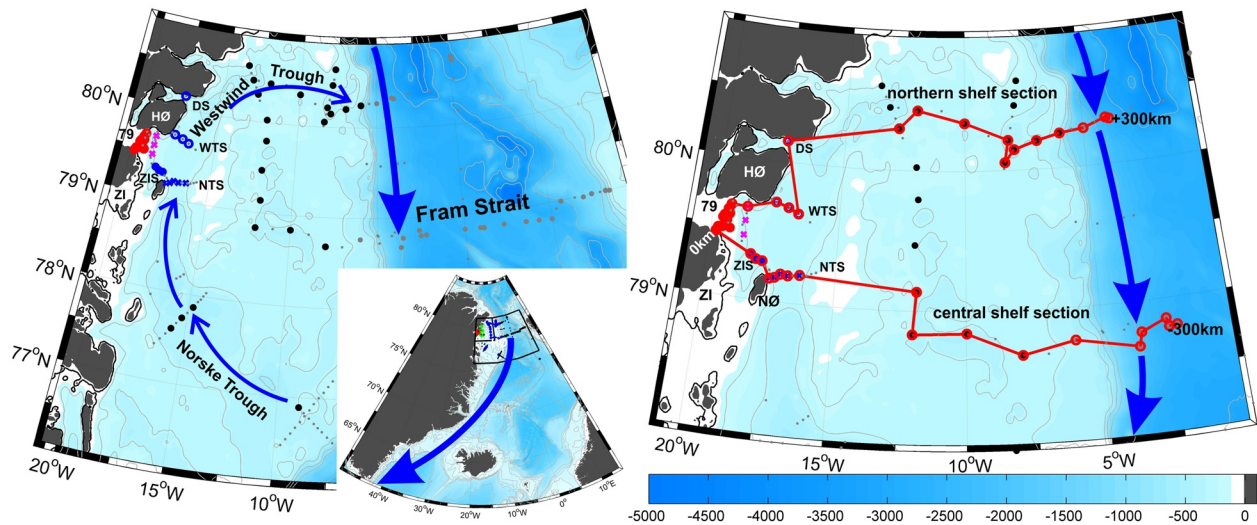
Figure 1. Map of R/V POLARSTERN expedition PS100, 2016. Bathymetry in blue shading. Gray lines indicate isobaths (4,000, 3,000, 2,000, 1,000, 750, 500, 250, 100), gray-shaded is above sea level, and thick black line indicates the ice edge. Bottom topography and ice edge based on ETOPO1 Global Relief Model (https://www.ngdc.noaa.gov/mgg/global/global.html; uploaded May 2011, downloaded November 2017). The thin blue arrows in the overview map (left) schematically indicate the mean clockwise circulation pattern on the shelf, the thick blue arrows represent the ECG. Small gray dots mark all CTD stations, thick dots mark stations with noble gas measurements. Gray dots are stations in Fram Strait; blue, magenta, and red indicate the proximity to the 79NG ice shelf front. This color scheme is maintained in the following figures. The red line in the zoomed map (right) shows the geographical position of the sections presented below. This path has been chosen to include most of the noble gas stations. Abbreviations of geographical features and sub-sections in clockwise order: NTs = Norske Trough section, NØ = Norske Øer, ZI = Zachariæ Isstrøm, ZIs = Zachariæ Isstrøm section, 79 = Nioghalvfjerdsfjorden Glacier (79NG), HØ = Hovgaards Ø, WTs = Westwind Trough section, DS = Dijmphna Sund.

(SMW) above the identification threshold fraction of 0.075% is mostly confined in the upper 400 m in the boundary current, while it could not be detected in the interior of the basins (Rhein et al., 2018).

The major sources of Greenland SMW are in northern Greenland. Here, the Nioghalvfjerdsbræ (referred to as 79 North Glacier, 79NG, Figure 1) is the largest of three marine-terminating outlet glaciers of the Northeast Greenland Ice Stream (NEGIS), whose drainage basin represents more than 15% of the GrIS area (Rignot & Kanagaratnam, 2006). While losing mass (Mayer et al., 2018; N. Wilson et al., 2017), the 79NG still maintains a floating ice tongue of about 80 km length and a main calving front of about 20 km width. The main ice shelf front is split by shallow bedrock highs in several channels (Mayer et al., 2000). The cavity below the ice shelf is up to 900 m deep near the grounding line and shallows toward the calving front. To the north, the 79NG calving front terminates at the Hovgaards Ø (HØ). A second smaller front (8 km width) has its outlet into the Dijmphna Sund, west of HØ.

Warm and saline water of Atlantic origin, named AIW (Atlantic Intermediate Water, $\theta > 1°C$; e.g., Budéus & Schneider, 1995); enters the Northeast Greenland Shelf mainly through Norske Trough (Figure 1) and, following a clockwise pathway, reaches the 79NG (Schaffer et al., 2017). A sill of about 325 m depth is sufficiently deep to allow AIW to enter the cavity below the floating ice tongue (Schaffer et al., 2020). In the cavity, the heat of the AIW melts the floating ice at the base of the ice tongue, cooling and freshening the water. Based on ocean time series measurements at the calving front, Schaffer et al. (2020) used the AIW heat transport to calculate a SMW flux of 0.56 ± 0.17 mSv (1 mSv = 10^{-3} Sv = 10^3 m³/s). Additionally, about 11% subglacial runoff of surface meltwater is added to the mix (Schaffer et al., 2020). The colder and fresher outflow from below the tongue is exported with the clockwise circulation northeastwards in the Westwind Trough toward the shelf break and will presumably be transported south with the East Greenland Current (EGC).

Another NEGIS outlet glacier, the Zachariæ Isstrøm located just south of the 79NG (Figure 1), has already lost most of its floating ice tongue, and calving takes place at the grounding line (Mouginot et al., 2015). Under global warming, this fate is also expected for the 79NG (Choi et al., 2017). For now, the 79NG ice

tongue has lost about 30% of its thickness due to increased submarine melting, and the grounding line has retreated inland by about 2 km between 1998 and 2014 (Mayer et al., 2018).

Changes in front of 79NG and Zachariæ Isstrøm have also been observed: Since the 2000s, the former perennial Norske Øer Ice Barrier (NØIB) that abuts the 79NG and Zachariæ Isstrøm breaks up in summer almost each year (Sneed & Hamilton, 2016), which was a rare event before the 2000s. The area of the NØIB is variable. For instance, in June 2012, the NØIB extended 140 km east of the 79NG and 375 km in the meridional direction (Sneed & Hamilton, 2016). Now, the NØIB consists mainly of first-year ice (Sneed & Hamilton, 2016). To the north, at about 79.5°N, the Northeast Water (NEW) Polynya is located and generally opens in spring and could reach from the Greenland coast to about 10°W (e.g., Minnett et al., 1997; Schneider & Budéus, 1997; Syring et al., 2020).

Once leaving the ice shelf cavity, freshwater from submarine melting is indistinguishable from other freshwater sources by salinity alone. The noble gases helium (He) and neon (Ne), however, provide a unique way to detect and quantify the SMW fractions. The SMW from Greenland is usually named SMW in the literature (N. Beaird et al., 2015; Rhein et al., 2018), and we will continue to do so in this manuscript. In Antarctic studies, submarine (basal) meltwater is usually named Glacial (basal) Melt Water (GMW, e.g., Huhn et al., 2018). The noble gas method was first used to trace SMW from Antarctic ice shelves (Hohmann et al., 2002; Huhn et al., 2008, 2018; Schlosser, 1986; Weppernig et al., 1996). For instance, analysis of noble gas data taken below the Filchner Ronne Ice Shelf resulted in an average basal melt rate of 177 ± 95 Gt per year, confirming earlier estimates from other data and methods (Huhn et al., 2018). N. Beaird et al. (2015) and N. L. Beaird et al. (2018) applied the noble gas method in Greenland fjords, and Rhein et al. (2018) were able to follow SMW in the boundary current from the southern tip of Greenland to the Canadian coast at 53°N. Combining these data with boundary current velocities, they found that SMW around Cape Farewell accounts for 12 ± 6% of the total east Greenland freshwater flux.

Here, we analyze He and Ne data that have been collected in Fram Strait and on the Northeast Greenland Shelf during the R/V Polarstern expedition PS100 (July–September 2016, Figure 1). We quantify and highlight the distribution of SMW from the source at the 79NG ice tongue to Fram Strait and discuss the implied circulation. Some of the SMW contains crustal He due to previous contact of the melting ice with the bedrock, providing more indications of the spreading and source of SMW. We also elucidate the distribution of anomalous low He/Ne ratios observed in the upper 100 m of the water column that are caused by Ne-enriched brine release during sea ice formation. After presenting the data, the processes that affect the He and Ne concentrations are listed, followed by the methods to calculate SMW fractions and sea ice formation. Results and discussion encompass the circulation of SMW, its formation rate, the ventilation time of the Northeast Greenland Shelf, and the rate of sea ice formation.

2. Data and Methods

2.1. Noble Gas Measurements

During the R/V POLARSTERN expedition PS100 in summer 2016 (19 July to 9 September) we took 650 water samples from 69 stations to analyze the stable noble gas isotopes ^{3}He, ^{4}He, ^{20}Ne, and ^{22}Ne in Fram Strait, on the Northeast Greenland Shelf, and near the 79NG (Figure 1). In 2016, the NØIB broke up in time to allow us to sample directly in front of the 79NG (red dots and magenta crosses), so the main 79NG ice shelf front could be well resolved by noble gas data. Close to the second, smaller calving front into the Dijmphna Sund, only one He/Ne profile above 100 dbar is available.

The He and Ne samples were collected from the CTD/water bottle system into gas-tight copper tubes and analyzed in the noble gas mass spectrometry lab Helis (Sültenfuß et al., 2009) at the University of Bremen. In a first step, the copper tube water samples were processed with an ultra-high vacuum gas extraction system. Sample gases were transferred via water vapor into a glass ampoule kept at liquid nitrogen temperature. For analysis of the noble gas isotopes the glass ampoules were connected to a fully automated ultra-high vacuum mass spectrometric system equipped with a two-stage cryogenic trap system. The system is regularly calibrated with atmospheric air standards (reproducibility better ±0.2%), and measurements of blanks and linearity are carried out (Sültenfuß et al., 2009). Finally, 515 valid measurements are used here. Based on replicate samples, the uncertainty of He and Ne is ±0.4%.

For the transient tracers (chlorofluorocarbons, CFC-11 and CFC-12), a total of 740 samples at 61 stations were collected. Water samples were transferred from the CTD-rosette-system into glass ampoules avoiding atmospheric contact. The ampules were flame sealed after a tracer-free headspace of purified nitrogen was applied. The samples were analyzed by purge and trap pre-treatment followed by gas chromatographic (GC) separation on a capillary column and electron capture detection (ECD) (Bulsiewicz et al., 1998). The total error of the measurement is ±1.5% for CFC-11, and ±1.0% for CFC-12. Only the samples taken along the 79NG ice shelf front are summarized in a mean profile and used here.

Processed hydrographic data from the R/V POLARSTERN expedition PS100 were downloaded from Pangaea (https://doi.org/10.1594/PANGAEA.871028) and published in Schaffer (2017).

2.2. Processes Affecting Noble Gas Isotopes in Seawater

In the ocean, the stable isotopes ^{3}He, ^{4}He, ^{20}Ne, and ^{22}Ne are abundant. The processes studied in this manuscript, however, involve only the total He and Ne. Henceforth, He and Ne is used instead of the main isotope ^{4}He, and "total" Ne. The main source of oceanic He and the only source for Ne is the gas exchange with the atmosphere. In general, He and Ne concentrations in the ocean exhibit an oversaturation of a few percent due to, for instance, wave breaking and gas bubble injection (e.g., Loose & Jenkins, 2014; Well & Roether, 2003). This oversaturation is maintained in the ocean interior and taken as a background value for all water masses that are not affected by the processes listed in the following.

Input of He and Ne by submarine melt: Atmospheric air with a constant composition of the noble gases He and Ne is trapped in the ice matrix during formation of the meteoric ice. When the ice is melting at depth or at the ice shelf base inside an ice shelf cavity, these gases are completely dissolved in the water, due to the enhanced hydrostatic pressure. This leads to an excess of ΔHe = 1280% and ΔNe = 890% in pure SMW (Loose & Jenkins, 2014); the Δ stands for the gas excess over the air-water solubility equilibrium,

$$\Delta C = 100 * \left(C^{obs}/C^{eq} - 1 \right) \left[\% \right] \tag{1}$$

Melting at the surface of the glacier or the ice shelf would equilibrate quickly with the atmosphere and does not show a noble gas excess in ocean water.

SMW with crustal He: SMW may be additionally enriched in crustal He (i.e., the isotope ^{4}He) from α-decay of uranium, thorium, and their daughter products in the bedrock beneath the ice sheet. On geological timescales, the crustal He accumulates in the overlying ice up to 300 m above the bedrock (Bieri et al., 1964; Craig & Scarsi, 1997; Suess & Wänke, 1963). There, He can be enriched 3–4.5 times compared to pure SMW (Craig & Scarsi, 1997; Jean-Baptiste et al., 2001). The exact ratio depends on the composition of the bedrock and the time the ice has been in contact with it. Crustal He enriched SMW detected by anomalous high He/Ne ratios have, for instance, been found in the water column below the Filchner Ice Shelf (Huhn et al., 2018) but not in the data around the southern tip of Greenland (Rhein et al., 2018). To separate the crustal He excess from the equilibrium concentration, the observed concentration ratios are normalized by the equilibrium concentration ratios as

$$\Delta \left(He/Ne \right) = 100 * \left(\left[He^{obs}/Ne^{obs} \right] / \left[He^{eq}/Ne^{eq} \right] - 1 \right) \left[\% \right] \tag{2}$$

In Fram Strait, that is, far away from crustal He sources, we found a mean Δ(He/Ne) of 1 ± 0.5% (standard deviation of the data). We identify water with Δ(He/Ne) > 2% (i.e., the mean of the ratio in Fram Strait of 1% plus two times the uncertainty of 0.5%) to be significantly enriched with crustal He.

Subglacial runoff: Part of the subglacial runoff is thought to be meltwater from the surface of the ice sheet, that flows through crevasses until it arrives at the base of the ice sheet. Some of it reaches the grounding line of the ice tongue, discharges into the ambient water, and joins the mix of AIW and SMW. Under the assumption that the subglacial runoff is equilibrating its noble gas content with the atmosphere before descending, and assuming that it does not pick up any noble gases on its way to the grounding line and into the cavity, it would not show a notable He or Ne excess and thus not be part of the SMW presented here. The time from the surface melt of the ice sheet to the grounding line is presumably short—Das et al. (2008)

found that a descent from the surface to 980 m depth in the GrIS needed about 2 h–so that the latter assumption is most likely valid.

A further part of the subglacial runoff is meltwater produced at the base of the ice sheet by geothermal or frictional heating. This part of the subglacial runoff can be contaminated with crustal He. However, this crustal He signal is not unique. The ice within 300 m above the base of the ice sheet could also contain crustal He. The measurement available to us do not allow to separate the crustal He signal of subglacial runoff from the crustal He signal present in SMW. In our approach, crustal He added by subglacial runoff is included in SMW, whereas subglacial runoff from the surface of the ice sheet cannot be quantified from our observations.

Formation and melting of sea ice: Due to their different atomic weights, He/Ne ratios in ocean water are affected by sea ice formation and sea ice melting (Hahm et al., 2004). Sea ice rejects salt and substantial amounts of Ne, while He is incorporated into sea ice. As a consequence, brine is enriched in Ne and leads to anomalous low He/Ne ratios in seawater including brines. Analog to crustal He, we assume Δ(He/Ne) < 0% (i.e., the mean background minus two times the confidence interval) to be significantly enriched with Ne from brine rejection. The Ne excess is maintained in the water, that gets denser by the extra salt, and the sea ice prevents gas exchange with the atmosphere. During sea ice melt, Ne reduction is small and restricted to a shallow mixed layer, where air-sea gas exchange quickly equilibrates the noble gas concentrations. So, in contrast to sea ice formation, sea ice melting is hardly detectable with noble gas data.

2.3. Calculating SMW Fractions

To calculate the SMW fraction in each sample from He and Ne data, we use the method from Rhein et al. (2018). To exclude the natural oversaturation that is almost ubiquitous in ocean water (e.g., Loose & Jenkins, 2014), the mean noble gas excess in the mixed layer $\Delta C^{\text{surf-excess}}$ far away from the 79NG is subtracted from all measured values. From stations in Fram Strait with a water depth >2,000 m and sample depths <20 m, we found a mean $\Delta He^{\text{surf-excess}}$ = 5.1 ± 0.8% and $\Delta Ne^{\text{surf-excess}}$ = 4.3 ± 0.7%. The uncertainty given is the standard deviation of the surface excesses. These values are similar to those reported by Rhein et al. (2018) for data collected south of Greenland (5.0 ± 0.52% for He and 4.1 ± 0.65% for Ne). We then subtracted the equilibrium value from each sample, using the solubility function $C^{\text{eq}} = f(T,S)$ from Weiss (1971). The remaining concentration is finally attributed to the presence of pure SMW with He = 26.189 nmol/kg and Ne = 88.739 nmol/kg (e.g., N. Beaird et al., 2015). The measurement error of ±0.4% for each of He and Ne results in an error of the SMW fractions of ±0.03%. The largest uncertainty in calculating SMW is the variability of the He and Ne surface excesses. To get an upper bound, we choose this uncertainty to be ±1.25%, that is, about 1.5 times the observed standard deviation. In combination with the much smaller measurement error this results in an overall uncertainty of the calculated SMW fractions of 0.1%. Only SMW fractions higher than this value are judged to be significant.

2.4. Calculating Sea Ice Formation From Ne Enriched Brine Release

When sea ice is formed, its releases additional Ne and lowers the He/Ne ratio in the remaining seawater. For the calculation of the fraction of sea ice to the initial water we followed the approach from Hahm et al. (2004), who used the sea ice/seawater partition coefficients for He p_{He} = 1.12 ± 0.15 and for Ne p_{Ne} = 0.66 ± 0.14. The fraction of ice f_i, that is, of the water frozen to sea ice from the initial seawater is calculated as

$$f_i = \left(C_o \, / \, C_w - 1 \right) / \left(p - 1 \right) \tag{3}$$

with C_0 being the initial noble gas concentration the water would have before sea ice formation, and C_w is the measured noble gas concentration in the residual water after sea ice formation. This implies that, for example, by a sea-ice formation of 10% of the initial water, the remaining seawater would gain 3.5% Ne and lose 1.2% He.
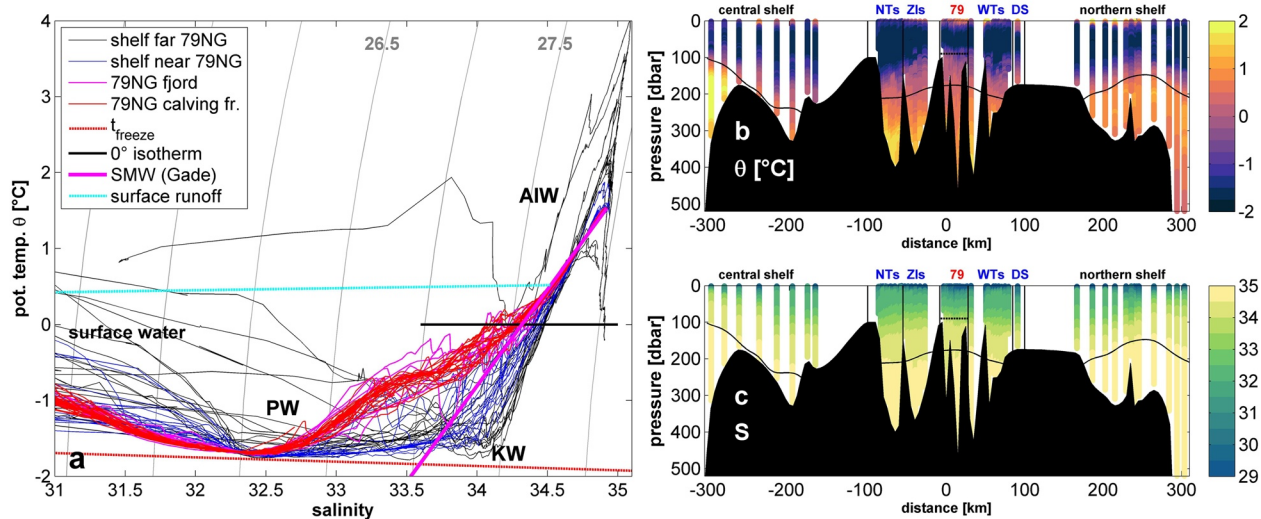
Figure 2. Salinity S and potential temperature θ from August 2016 (cruise PS 100). 2a: θ-S-diagram color coded similar as in Figure 1. Red line = surface freezing temperature. Black line = 0°C isotherm as boundary between AIW and PW (Aagaard et al., 1985; Korhonen et al., 2013), blue line = mixing line with subglacial runoff, magenta line = GADE line (see text). Gray curves = isopycnals σ_θ = 25.0:0.5:28.0 kg/m³. Panel b shows θ and Panel c shows S distributions along the section shown in Figure 1. The thin black line highlights the 0° isotherm. Black dashed line = underside of the 79NG ice shelf front.

3. Results

3.1. Temperature and Salinity Distribution

The upper-ocean water masses in Fram Strait and on the Northeast Greenland Shelf are a mix of warm and saline Atlantic Water and less dense cold and fresh Polar Water (PW) (Schaffer et al., 2017). On the shelf, after being subducted below the PW, the Atlantic Water is named AIW. On the shelf, AIW potential temperatures of up to 2.7°C have been observed and the potential temperature minimum of PW was −1.8°C (Figure 2). Knee Water (KW) is a water mass which is advected onto the shelf from Fram Strait and has temperatures close to the freezing point and salinities near 34 (Bourke et al., 1987; Budéus & Schneider, 1995). This water mass is formed by sea ice formation in the Arctic Ocean. It is found in Norske Trough while its signature is diminished further downstream on the shelf.

Close to the calving front, the AIW displayed maximum temperatures of 1.52°C in August 2016 (red profiles in Figure 2a). Warm AIW flows into the ice shelf cavity and induces submarine melting (Schaffer et al., 2020). The maximum AIW temperature below the floating ice tongue that was measured by moored instruments at 500 m depth was 1.5°C in July 2017 (Lindeman et al., 2020).

According to Schaffer et al. (2020), the outflow from the 79NG cavity is above 250 m depth and has a maximum at about 120 m, slightly below the underside of the ice tongue at 90 m depth. In front of the tongue, the T/S characteristic of the outflow warmer than 0°C follows the melt-freeze line (Gade line; see Gade, 1979; Jenkins, 1999). The Gade line is the mixing line between pure SMW (salinity = 0, effective temperature accounting for the latent heat of melting = −87°C) and the warm ambient AIW (θ = 1.52°C, S = 34.92). Water with lower temperatures at that location is fresher than the Gade line. The profiles named "79NG fjord" (magenta profiles in Figure 2a) show the largest freshening relative to the Gade line, followed by the stations directly in front of the 79NG and by stations in the Zachariæ Isstrøm domain. The deviation from the Gade line toward lower salinities is by mixing with subglacial runoff (N. J. Wilson & Straneo, 2015) and, further away from the calving front, with PW. The density threshold below which the profiles deviate from the Gade line by mixing with subglacial runoff is at about the σ_θ = 27.7 isopycnal (Schaffer et al., 2017). As shown below, this isopycnal is the densest water that has significant fractions of SMW.

The sequence of stations (Figure 1, red line in the right map) in Figures 2b and 2c and following sections is chosen to encompass most of the noble gas stations. The section starts at the continental shelf break at 79°N (−300 km) and extends the Fram Strait section over the central shelf toward the west. The stations east of the Zachariæ Isstrøm form a section across the Norske Trough. It is followed by the Zachariæ Isstrøm
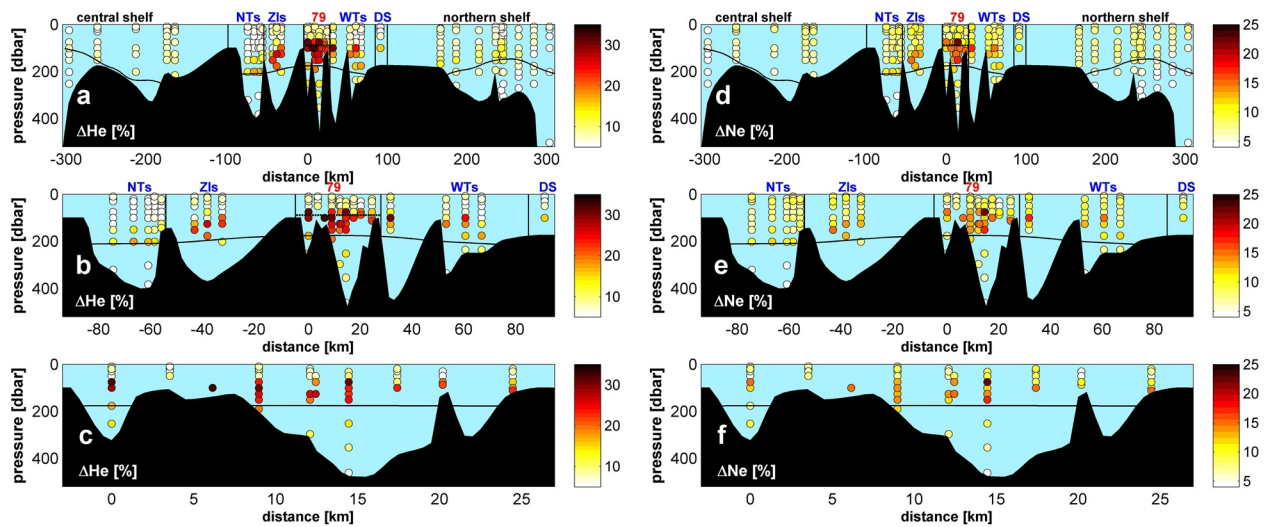
Figure 3. He (left) and Ne (right) supersaturations along the sections highlighted in the map in Figure 1 (a and d); zoom into the sections from −90 km downstream to 90 km upstream of the 79NG calving front (b and e); zoom along the 79NG calving front (c and f). Black lines mark the depth of the 0°C isotherm, chosen as a boundary between warm AIW and colder PW.

section along the Zachariæ Isstrøm outlet and the stations close to the 79NG main calving front. Next comes a section across the southern entry of the Westwind Trough just northeast of the 79NG main calving front, one station inside the Dijmphna Sund, and further stations along the northern shelf at 80.5°N toward the shelf break (300 km). The 0°C isotherm was chosen as the boundary between AIW and PW. All sections presented here follow this sequence of stations.

The depth of the 0°C isotherm is 100 dbar in Fram Strait compared to 250 dbar on the southern shelf where PW is more abundant. In the Zachariæ Isstrøm region and at the 79NG calving front, the isotherm rises to about 180 dbar, most likely because they are located in or close to the Norske Trough, where the main inflow of AIW toward the 79NG occurs (e.g., Schaffer et al., 2017). Salinities below $S = 33$ are confined to the upper 50 dbar of the water column on the eastern part of the shelf, and reach down to about 80 dbar in the western parts of the section. In the Norske Trough section the 0°C isotherm is much deeper due to the abundance of KW. Close to the coast the 0°C isotherm is shallower due to modified AIW (mAIW) by meltwater.

3.2. Helium and Neon

Away from sources, He and Ne have a background supersaturation in the Fram Strait of 5.1% for He and 4.3% for Ne. We found much higher He and Ne supersaturations all over the shelf (Figure 3), with the highest excesses (up to 34.4% for He and up to 22.1% for Ne) in front of 79NG (Figure 3), confirming the 79NG as the source of SMW. The strongest noble gas signals are observed in water at or above the 0°C isotherm, confined to depths below 100 dbar (i.e., roughly the depth of the glacier base at the calving front). In front of the 79NG calving front, noble gas excesses partly reach up to the surface. The southern part of the ice shelf front (km 0–6) exhibits the highest He supersaturation. This feature is not matched by Ne, so we interpret it as a distinct path of crustal He enriched meltwater. In the upper 100 dbar, Ne anomalies are found to be larger at many shelf stations, while the He anomalies are small. We attribute this being caused by Ne enrichment in the brines rejected during sea-ice formation.

To disentangle the influence of crustal He and of Ne from sea-ice formation, all He-Ne pairs are displayed in Figure 4. The magenta ellipse represents the background He-Ne pairs defined from stations in Fram Strait away from the shelf. They characterize all water masses in the study area without SMW, crustal He, or sea ice formation. The He-Ne pairs only affected by SMW should follow the mixing line from this background ratio toward pure SMW (thick solid magenta line). Most of the He measurements at the 79 NG calving front (red dots) and in the fjord (magenta x) show a strong deviation from the SMW mixing line toward higher He excesses; that is, crustal He contributions. We assume that pure crustal He-enriched melt water contains
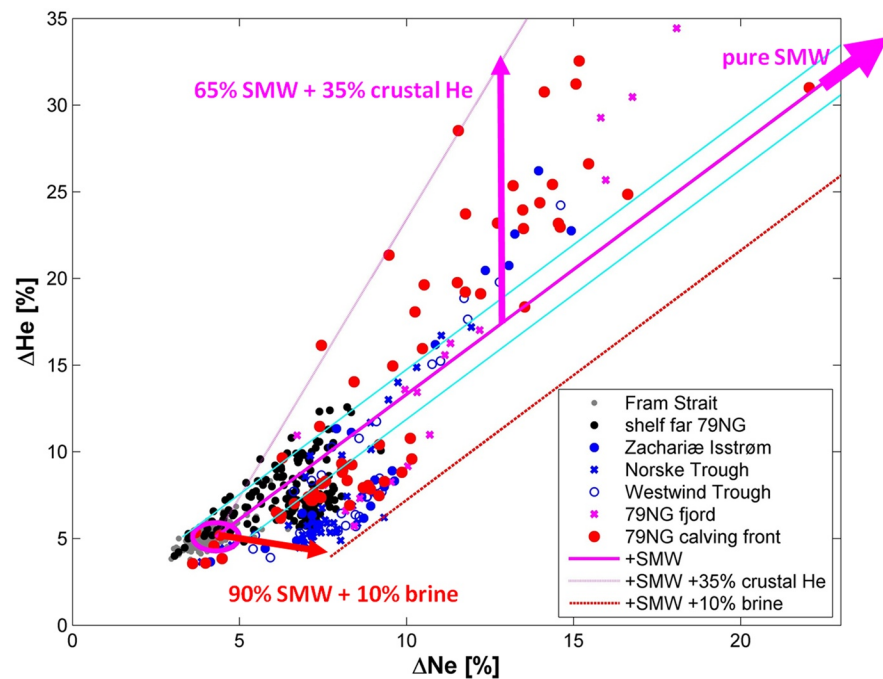
Figure 4. Observed Ne and He excess (color coded as in Figure 1). The thick magenta line is the mixing line between the background (the magenta ellipse) and pure (100%) SMW. The background was chosen as the mean He and Ne surface water excess in Fram Strait stations and their uncertainties (ΔNe = 4.3 $\pm$ 0.7%, ΔHe = 5.1 $\pm$ 0.8%). The light magenta line is the mixing line between the background and a mix of 65% SMW and 35% meltwater with crustal helium addition (see text). The red line is the mixing line between the background and SMW with Ne enriched brine addition by sea ice formation. The offset from the thick magenta SMW mixing line represents a transformation of 10% of the initial water mass to sea ice. The thin cyan lines indicate significance limits for Ne enrichment from sea ice formation and crustal He enrichment (see text above).

4.5 times more He than the air bubbles in the ice (Craig & Scarsi, 1997), and the largest He deviations correspond then to a fraction of 35% crustal He enriched melt water in SMW (light magenta line in Figure 4).

A large number of He-Ne pairs from the upper 100 dbar on the shelf are shifted toward higher Ne excesses, suggesting the presence of water modified by sea ice formation. The smaller shift of samples toward higher Ne excesses at the southern and central shelf (black dots) compared to closer to 79NG (red, magenta, blue) indicate that the latter samples are more affected by sea ice formation. The maximum Ne deviation of +3.5% corresponds to 10% of the original water mass being transformed to sea ice (Figure 4, red line). However, most samples show lower Ne deviations corresponding to 4%–8%. In front of the 79NG, the crustal He could obscure the weaker effect of elevated Ne by sea ice formation. For most of the other samples the signals from crustal He in SMW and from Ne enriched brine from sea ice formation are separated sufficiently: crustal He is found below 75 dbar (Figure 5a) while the sea ice formation signal is mainly confined to the upper 100 dbar (Figure 5b).

3.3. SMW Fractions

The noble gas observations reveal the presence of crustal He in many samples (Figure 5b). Crustal He increases He but has no effect on Ne. On the other hand, we found samples with Ne addition from sea-ice formation, leading to higher Ne concentrations (Figure 5a). To minimize the positive biases on SMW fractions from crustal He from elevated Ne through sea ice formation, we will use in the following the smaller SMW fraction calculated from Ne or He, respectively (Figure 6). Ne added during sea-ice formation is evident in the upper 100 dbar, whereas crustal He contributions are found in the layers below (Figure 5) making it unlikely that both effects overlay each other. A loss of He by sea ice formation in the upper 100 dbar is small (10% sea ice formation results in a loss of 1.2% He, which is equivalent to ~0.07% SMW). We neglected this small effect in the SMW calculations.
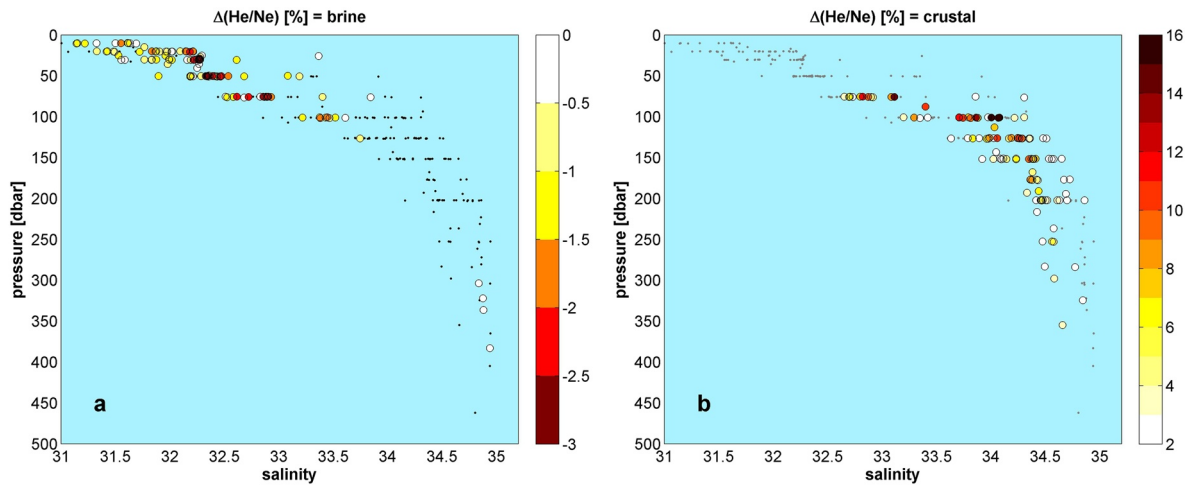
Figure 5. (a) He/Ne ratio, color dots show significant Ne excess (Δ(He/Ne) < 0%), indicating sea ice formation. Small black dots are all other data points on the shelf without significant Ne enrichment by sea ice formation. (b) He/Ne ratio, color dots show significant He excess (Δ(He/Ne) > 0%), indicating crustal He addition. Small black dots are all other data points on the shelf without significant crustal He signal.

The maximum SMW fractions (up to 1.8%) are observed slightly below the base of the 79NG ice tongue between 80 and 150 dbar (Figure 6). Maximum SMW fractions are most evident directly at the 79NG calving front (79NG calving front, red dots in Figures 4 and 6) and in section 15°km offshore (79NG fjord, magenta x).

Further away from the 79NG, the maximum SMW fraction is located deeper (between 100 and 200 dbar) in the water column (Figure 6c). Significant SMW fractions are found all over the shelf with decreasing amplitudes with distance from the source (Figure 7). In the Westwind Trough on the northern part of the shelf, the SMW fractions remain higher, but fade at the shelf break (Figure 7), supporting the observations suggesting a clockwise shelf circulation at all depths. Significant SMW fraction were not found east of the shelf, neither in the central shelf section at 79°N nor further north at the exit of the Westwind Trough (Figure 7).

The SMW profiles within 90 km distance from the 79NG are shown in Figure 8. High SMW fractions along the 79NG calving front (red dots) and at the 79NG fjord section (magenta x) are spread over a wide depth (Figure 8a) and density range (Figure 8c), with SMW > 0.7% between σ_θ 26.0 and 27.7 kg/m³. At stations along the Zachariæ Isstrøm (blue dots) and Norske Trough (blue x), the SMW maximum is found about 25 m deeper in the water column and in more dense waters, with SMW > 0.4% below σ_θ = 27.1 kg/m³ (Zachariæ Isstrøm) and below σ_θ = 27.3 kg/m³ (Norske Trough). Additionally, elevated SMW fractions are found in a smaller depth and density range compared to the abundance at the 79NG ice shelf front. In both domains, the density limit is σ_θ = 27.7 kg/m³, similar to our observations at the 79NG. Along the Norske Trough section, SMW in water less dense than σ_θ = 27.1 kg/m³ is below the significance limit. These stations are presumably upstream of the SMW source. The larger distance to the source is reflected by the more homogeneous nature of the SMW profiles.

Closer to the 79NG, the stations differ much more individually in their SMW maxima and the density range of the maxima. At the Zachariæ Isstrøm section, the significant SMW fractions (up to 0.3%) are observed in the upper water column with densities smaller than σ_θ = 26.1 kg/m³. On the Westwind Trough section (blue o), the profiles still have higher SMW fractions over a larger part of the water column (SMW >0.7% between σ_θ 26.6 and 27.6 kg/m³), but some of the shallower signal present at 79NG is already diluted (Figure 8c). At the northern shelf (cyan dots in Figures 8b and 8d) and at the southern and central shelf (black dots), that is, up to 300 km away from the 79NG, significant SMW fractions are apparent in most stations with maximum SMW fractions (up to 0.4%) at about σ_θ = 27.5 kg/m³. We find that the SMW fractions are higher over most of the water column on the northern shelf compared to the southern and central shelf. In Fram Strait, the SMW is diluted and below the significance level.

In short, the most robust SMW signal observed in summer 2016 on the NE Greenland shelf is between σ_θ = 26.5 and 27.7 kg/m³, encompassing the 0°C isotherm. The strong SMW maxima in front of the 79NG at
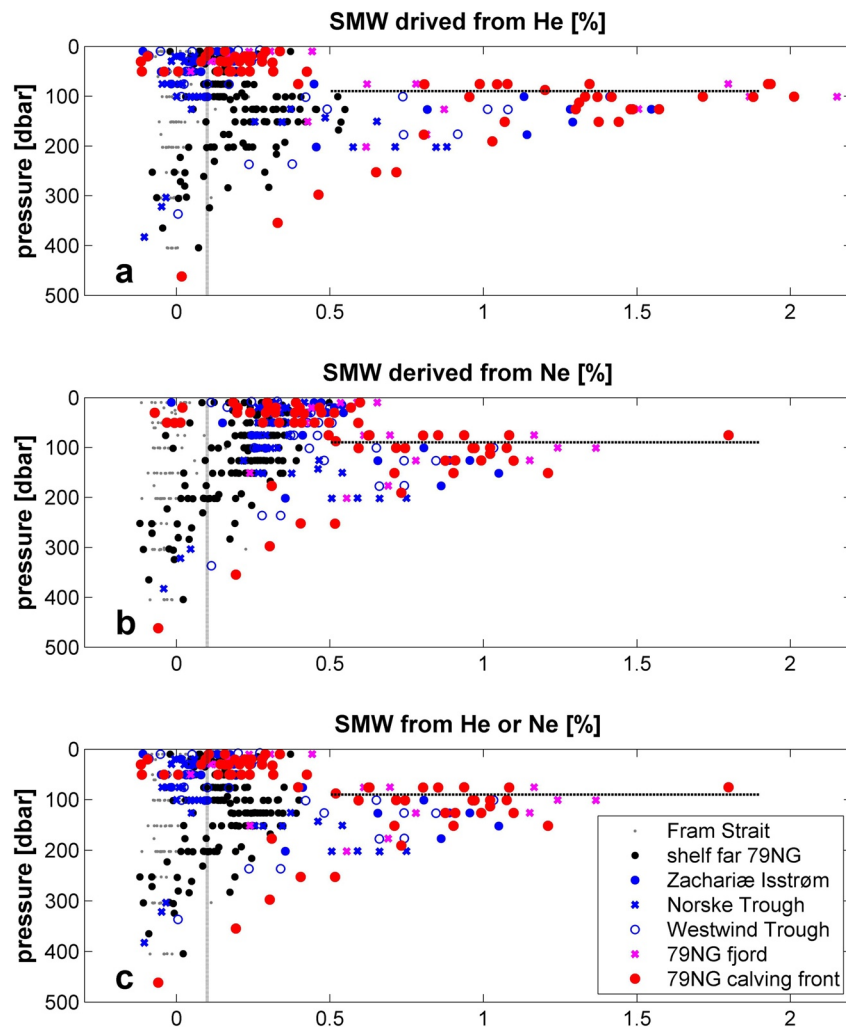
Figure 6. SMW fractions versus pressure from He (a), from Ne (b), and from He or Ne (whichever is smaller) (c). The horizontal lines indicate the depth of the underside of the 79NG ice shelf tongue at the calving front. The vertical line at 0.1% marks the significance limit.

shallower depths and lighter densities are eroded over short distances of roughly 60 km. This is elucidated by the difference in SMW fractions between the 79NG and the stations along Norske Trough, Zachariæ Isstrøm and Westwind Trough sections, where already parts of the shallower SMW maxima are missing. The persistence of the denser SMW signal indicates that either the volume of the shallower SMW modes is smaller than the denser modes and/or that the lateral mixing at these depths with ambient PW and KW is stronger. Nevertheless, some SMW remains present also in the water column above the SMW maximum. The spatial SMW distribution (Figure 7, map on the right) confirms that the SMW fractions are significant over most of the shelf, and larger on the northern compared to the southern and central shelf, which can be linked to the clockwise shelf circulation. At the shelf break and in Fram Strait, no significant amounts of SMW can be detected.

3.4. Crustal Helium

As for SMW, the 79NG is the source of crustal He on the Northeast Greenland Shelf (Figures 9a–9c). SMW with the strongest crustal He signal is observed in the southern part of the main 79NG calving front (0–10 km). The regional accumulation of crustal He at this location indicates a distinct meltwater pathway exiting the cavity, but velocity measurements point to very little outflow there (Schaffer et al., 2020). Crustal He is also found on the Westwind Trough section and on the northern shelf, deeper than directly at the ice
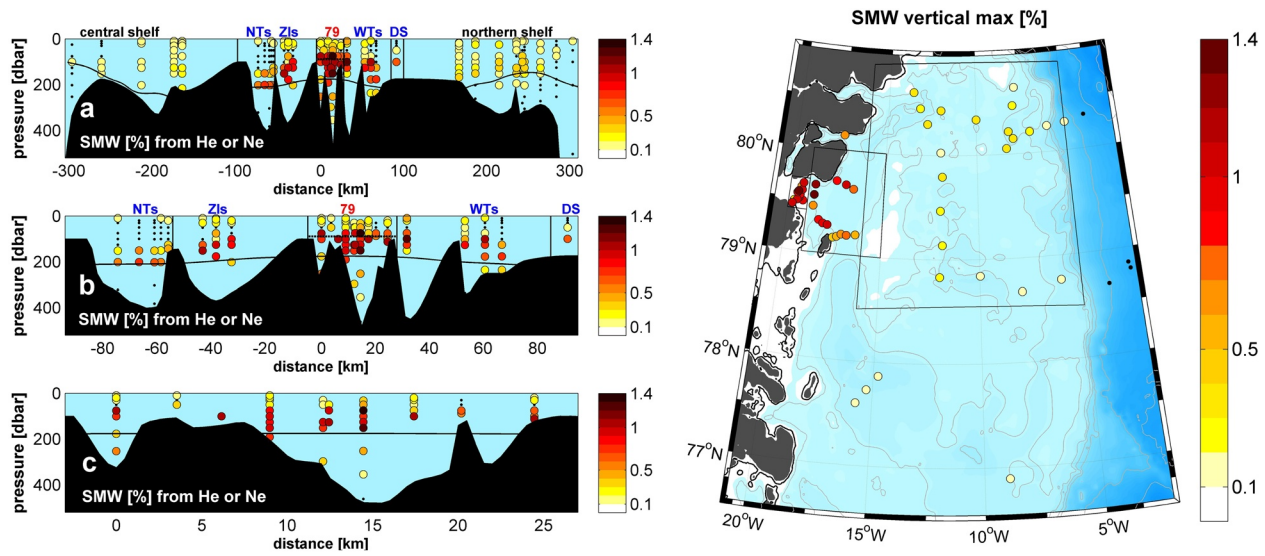
Figure 7. SMW section (left, a–c) and geographical distribution (right) of the SMW maximum (i.e., the maximum SMW fraction of each profile). SMW below significance limit of 0.1% are displayed as black dots. The black lines in the sections mark the 0°C isotherm. The light rectangles in the map indicate three sub-regions used for calculating SMW inventories below, Section 4.2.

shelf front and deeper than the maximum SMW signal. The crustal He signal follows the mean circulation pattern on the shelf, but fades out with distance to the 79NG. Some minor signal (2% < Δ(He/Ne) < 4%) is also present upstream of 79NG on the Norske Trough section (Figure 9a and map).

3.5. Ne Excess and Sea Ice Formation

The vertical distribution of low Δ(He/Ne) indicate the presence of Ne enrichment by sea ice formation almost everywhere on the shelf in the upper 100 dbar (Figure 10a). The strongest signal is observed along the Norske Trough and Westwind Trough sections, in the vicinity of the fast-ice cover and the NEW polynya, followed by the station at the Zachariæ Isstrøm section closest to the Norske Trough section. Further north and east of the Westwind Trough section, the signal first fades, but gets significant again at about +220 km at the northern shelf section area (Figure 10a). In the spatial distribution (Figure 10), Ne excesses due to sea ice formation are found in many stations. Besides the maxima along the Norske Trough, Zachariæ Isstrøm, and Westwind Trough sections, all stations north of 80°N and east of 12°W show elevated Ne levels.
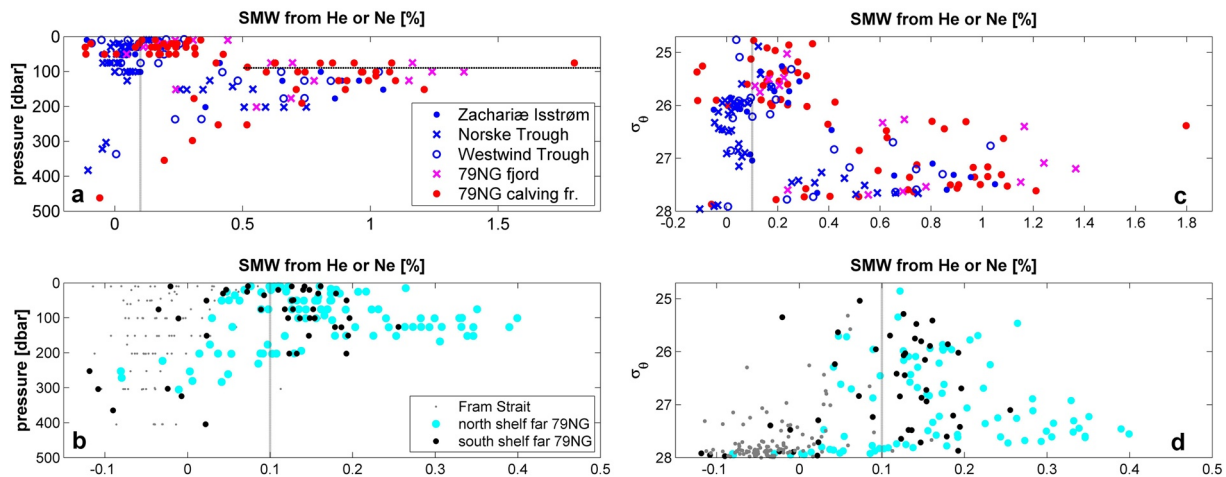
Figure 8. SMW fractions versus pressure, (a) separated for locations close to 79NG, and (b) for locations far off 79NG and in Fram Strait. And SMW fractions versus potential density, (c) separated for locations close to 79NG, and (d) for locations far off 79NG and in Fram Strait. Note the different scale of the x-axis.
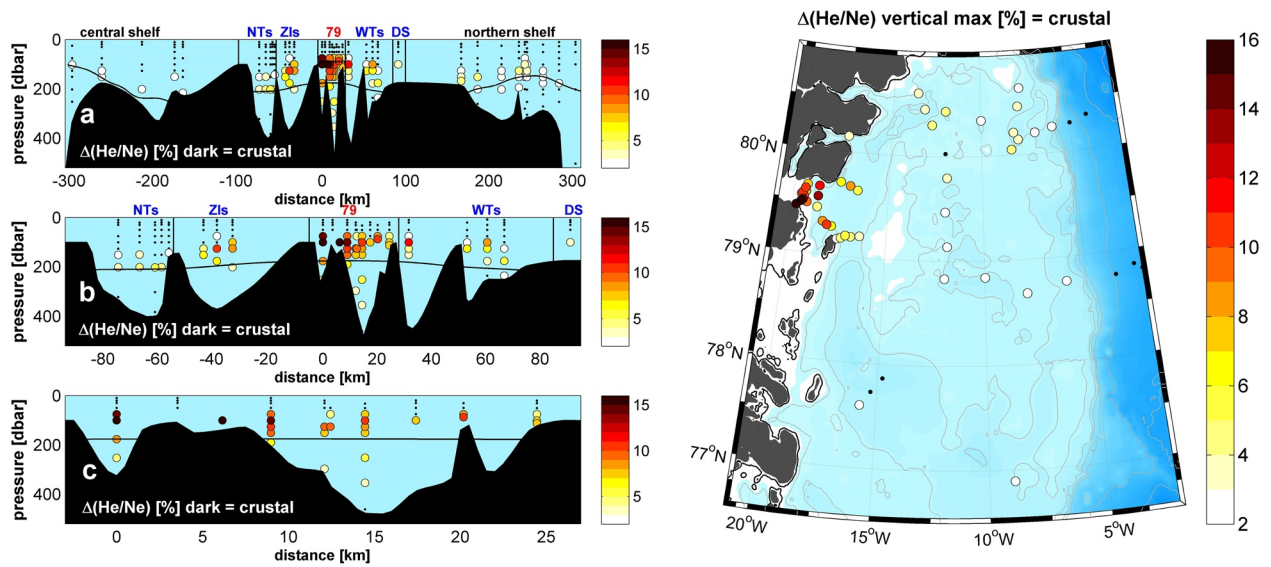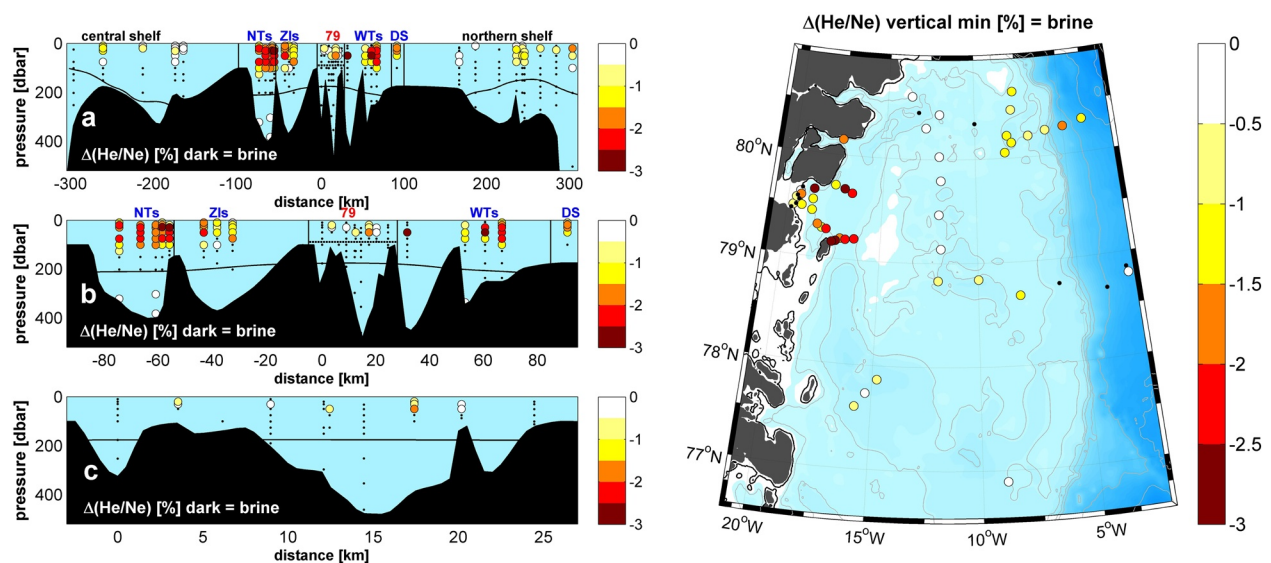
Figure 9. Crustal He expressed by high Δ(He/Ne). Left (a–c) the distribution along the section. The map shows the vertical maximum Δ(He/Ne) of each profile. Δ(He/Ne) > 2% is the significance limit for crustal He addition. Black dots are below the significance limit.

4. Discussion

4.1. Circulation of SMW

The main source of the SMW of the Northeast Greenland Shelf is clearly the 79NG. In front of the 79NG, high SMW fractions are found in the upper 230 dbar (Figures 7a–7c and 8a). The denser water (σ_θ = 26.5–27.7 kg/m³) with elevated SMW fractions reaches at least 60 km to the southeast to the Zachariæ Isstrøm domain and the Norske Trough section, as well as to the northeast (Westwind Trough section) and to the northern shelf (Figures 8c and 8d). The latter is expected, regarding the clockwise circulation following the trough system on the NE Greenland continental shelf (Bourke et al., 1987; Schaffer et al., 2017). However, the SMW profiles that follow the clockwise pathway toward the Westwind Trough downstream of the 79NG do not differ from the southeastern SMW profiles observed along the Zachariæ Isstrøm and Norske Trough sections, upstream 40 km to the southeast (Figure 8c, blue dots, x, o).

Figure 10. Ne anomalies from sea ice formation expressed by low Δ(He/Ne). Left (a–c) the distribution along the section. The map shows the vertical minimum Δ(He/Ne) of each profile. Δ(He/Ne) < 0% is the significance limit for Ne addition due to sea ice formation. Black dots are beyond the significance limit.
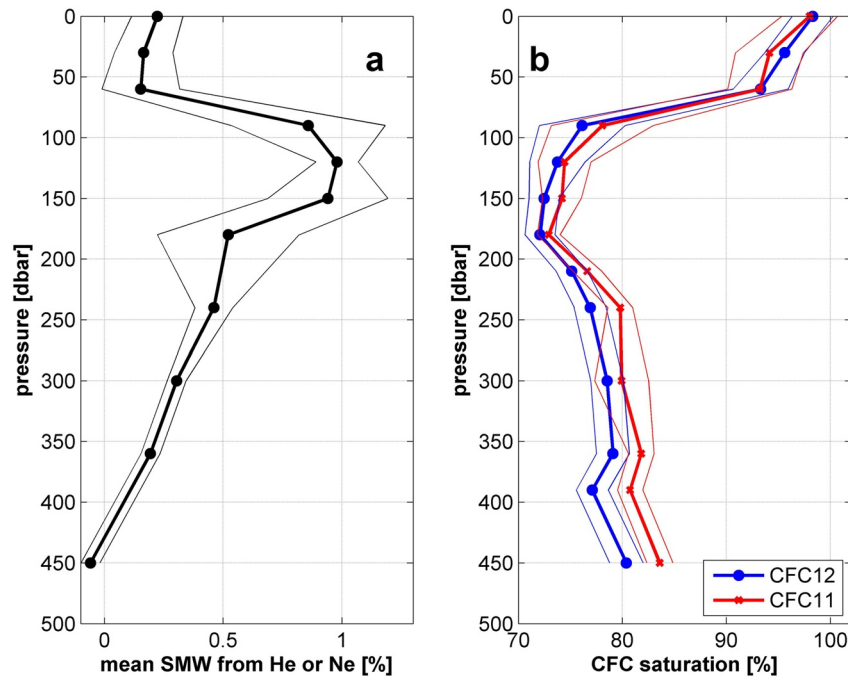
Figure 11. SMW fractions along the 79NG ice shelf front (a), averaged in 30 dbar intervals, and (b) CFC-12 and CFC-11 apparent saturations (i.e., observed vs. atmospheric partial pressure) along the 79NG ice shelf front, averaged in 30 m intervals. Bold lines are mean values within the vertical intervals and thin lines indicate their uncertainties (i.e., standard deviation of the SMW fractions or CFC saturations within the intervals).

We cannot entirely exclude that the SMW signal along the Zachariæ Isstrøm and Norske Trough sections originates from Zachariæ Isstrøm. This glacier has lost is floating ice tongue already (Mouginot et al., 2015), leaving only the calving front for SMW formation. The seafloor at its calving front is about 900 m deep and enables AIW to reach the ice cliff (Choi et al., 2017; Schaffer et al., 2020; Yang et al., 2020) and contact the rough surface of the cliff (Rignot et al., 2015). Another source of SMW could be the submarine melting of icebergs from the Zachariæ Isstrøm calving front in the fjord, that in former times held the ice tongue. In western Greenland fjords south of 79NG, submarine melting of icebergs contributes a large part to the freshwater budget (Enderlin et al., 2016). We suggest, that the 79NG is more likely the source of the observed SMW signals along the Zachariæ Isstrøm and Norske Trough sections. That implies a local additional southeastern pathway to the Zachariæ Isstrøm and Norske Trough sections for the SMW originating from the 79NG. This is also supported by the distribution of crustal He: the signal along the Zachariæ Isstrøm and Norske Trough sections most likely originates from the southernmost part of the 79NG ice shelf front, the domain of the main crustal He abundance.

Schaffer et al. (2020) found the smaller ice shelf front at Dijmphna Sund to be responsible for 45% of the SMW discharge and subglacial runoff from 79NG. One station with noble gas samples above 100 dbar is available so far at the Dijmphna Sund outlet. The moderate SMW signal is ambiguous; it could have been transported from 79NG with the main circulation through Westwind Trough. SMW at the northern shelf section could either originate from 79NG or Dijmphna Sund. The single station has no significant SMW fraction near the surface, but the SMW signal further north on the shelf points to the 79NG as the source. At the northern shelf break and east of it, the SMW fractions are small but remain significant (Figure 7), allowing a small portion of the SMW inventory to be exported with the East Greenland Current to the south. However, east of the shelf break of the central shelf section, no significant SMW fractions were detected.

4.2. SMW Formation Rate at 79NG and Ventilation of the Northeast Greenland Shelf

To calculate the SMW formation rate, all SMW profiles in front of the glacier tongue are averaged into a single vertical profile (Figures 11a). It shows a maximum SMW fraction between 90 and 150 dbar of 1.0 ± 0.1%. For the following calculation we assume that this represents the SMW fraction of the 79NG cavity outflow.

The cavity volume is 640 ± 80 km^3 covering an area 1.700 km^2 (Schaffer et al., 2020), and the overturning time of the cavity is 162 days or 0.44 years, based on velocity measurements in front of the cavity (Schaffer et al., 2020). The SMW formation rate is then estimated to be 14.5 ± 2.3 Gt per year. This is equivalent to a meltwater flux of 0.46 ± 0.07 mSv, or a melt rate for the 79NG of 8.6 ± 1.4 m per year. This estimate is comparable to the results from N. Wilson et al. (2017) of 13 Gt per year and to Schaffer et al. (2020) of 10.4 ± 3.1 m per year (Schaffer et al., 2020). If using the maximum observed SMW fraction in front of the 79NG calving front of 1.3% or 1.8% (Figure 8a), respectively, the submarine melt rate would be larger by 30% or 80%.

The shelf region with significant SMW fractions comprises roughly 41,250 km^2 (165 km from 79.0°N to 80.5°N, and 250 km from the 79NG calving front to the shelf break). If the SMW layer is 100 m thick (Figures 6 and 7) and the mean SMW fraction of that layer is 0.5%, the total amount of SMW would be 20.6 ± 1.5 km^3. Separating the shelf region into three sub-regions to take the dilution of SMW with distance from its source into account (Figure 7: close to 79NG with mean SMW = 1.05%, near field of 79NG with mean SMW = 0.66%, and far field of 79NG with mean SMW = 0.27%), the SMW inventory on the shelf is computed to 22.1 km^3. The SMW formation rate of 14.5 Gt per year implies that the shelf waters modified by SMW are ventilated every 1.4–1.5 years. This suggests that the conditions observed in late summer 2016 are representative of SMW production for the time period 2015–2016.

A significant loss of He and Ne at the ocean surface and, hence, calculating too low SMW fractions can be neglected in our case. Close to the calving front, SMW flowing out of the cavity could rise to the surface (e.g., Straneo et al., 2012) and thereby lose excess He and Ne to the atmosphere. However, the rather strong stratification (Figure 2) does not suggest upwelling and He and Ne loss as a relevant mechanism. CFC-12 profiles in front of the 79NG (Figures 11b) support this. The CFC saturation in the layer of the SMW maximum is around 70%, so upwelling of a substantial amount of SMW would decrease the CFC saturation in the mixed layer. The CFC saturation in Fram Strait is 99 ± 4%. Thus, the 98% CFC saturation observed in front of the 79NG calving front is within the uncertainty of an undisturbed mixed layer. Hence, a significant loss of CFC and of excess He and Ne to the atmosphere and an underestimate of SMW by this loss is negligible.

4.3. Sea Ice Formation

One hypothesis to explain the high Ne excesses (indicating sea ice formation) along the Norske Trough and Westwind Trough sections could be that they are advected with the clockwise circulation from Fram Strait. However, the stations in the Norske Trough closer to Fram Strait and in the Fram Strait itself, as well as the stations on the southern and central shelf, do not exhibit such a strong sea ice formation signal as in the Norske Trough and Westwind Trough sections (Figure 10). The Ne excess at these two locations seems to be mainly a local signal. Since 2000, the fast ice in front of NØIB mainly consists of first-year fast ice (Sneed & Hamilton, 2016), and the Ne excesses could have been released by sea ice formation since the breakup phase in 2016 and in the year before.

The northeastern patch of high Ne excesses could be a signal of sea ice formation in the NEW Polynya (e.g., Preußer et al., 2016). Considering the sea ice/seawater partition coefficient $p_{Ne} = 0.66 ± 0.14$ and the observed maximum Ne offset of +3.5% (see red line in Figure 4), we estimate a sea ice formation of 10% from the initial water $f_i = (C_o/C_w − 1)/(p − 1)$ or $0.1 = (1.000/1.035−1)/(0.66−1)$ (Equation 3). The high Ne excesses are found in the upper 100 m of the water column, so a mass percentage of 10% of frozen water corresponds to a sea ice formation of 9 m (assuming a sea ice density of 900 kg/m^3). Most samples, however, show a lower Ne excess equivalent to a sea ice formation (Figure 4), corresponding to a sea ice formation of about 6 m. Assuming that the ventilation time of the water on the shelf is 1.4–1.5 years as inferred from the SMW fractions, the yearly sea ice formation rate on the shelf would be 4 m. This seems fairly high for an area that is most of the year covered with fast ice. However, one has to take into account that most of the NØIB is only one year old and could be formed on the shelf. The NEW Polynya north of the Westwind Trough section covers an area of about 2,800 km^2 and forms, on average, about 22 ± 7 km^3 sea ice per year (Preußer et al., 2016), corresponding to a sea ice formation of 7 m per year.

5. Summary and Conclusions

A large part of the northeast Greenland shelf water is affected by noble gas excesses from submarine melting from the 79NG and perhaps the Zachariæ Isstrøm and, in the upper 100 m, from Ne excesses caused by sea ice formation. The noble gas excess is a unique characteristic of SMW. SMW fractions of up to 1.8% have been observed directly in front of the 79NG calving front. Part of this SMW is transported to the northeast by the predominantly clockwise circulation along the Westwind Trough, but there also seem to exist hitherto undetected pathways of SMW bearing water to the southeast of 79NG. We estimate a flushing time of the SMW modified shelf water of about 1.5 years from the SMW formation rate (14.5 Gt/year) and the SMW inventory on the shelf (about 22 km^3).

SMW is rapidly mixed with surrounding water on the shelf. At the shelf break, the SMW signal fades away (<0.1%) and is no longer detectable in the EGC and in Fram Strait. That makes it unlikely that SMW from the 79NG and other marine-terminating glaciers of Northern Greenland will influence the deep water formation regions in the eastern Nordic Seas, the Irminger Sea and the Labrador Sea in the near future. The SMW observed in the boundary current around the southern tip of Greenland (Rhein et al., 2018) consequently needs to be provided by marine-terminating glaciers south of 79°N.

The highest Ne excesses from sea ice formation have been observed in the Norske Trough and Westwind Trough sections southeast and northeast of 79NG. The Ne surplus in the troughs further upstream and downstream on the shelf and in Fram Strait is much smaller. This points to mainly local sea ice formation after the break-up of the NØIB fast ice in summer. The slightly elevated Ne excess to the northeast in and near the Westwind Trough might be affected by sea-ice formation in the NEW Polynya. On average, about 4 m of sea ice per year was formed on the Northeast Greenland Shelf.

In contrast to the Antarctic ice shelves, surface melting of the GrIS adds considerable amounts of freshwater into the ocean (Enderlin et al., 2014; Kjeldsen et al., 2015; Van Den Broeke et al., 2009). Surface melt is the main freshwater source in southern Greenland, although submarine melt also contributes (N. Beaird et al., 2015; Rhein et al., 2018). This needs to be accounted for when considering the role of GrIS mass loss on the circulation. To fully assess the role of SMW on the deep-water formation regions, the SMW flux from other Greenland marine-terminating glaciers and fjords needs to be estimated. New noble gas data on several sections across the East Greenland boundary current from 74°N to the Irminger Sea encompassing the main outlet glaciers have been collected and will be analyzed soon.

The interaction between SMW and Greenland glacier mass balance remains poorly understood and difficult to model (Beckmann et al., 2019; Mercenier et al., 2020). The response of the ocean to accelerated melt rates and thus freshwater input not only at the surface but also by SMW in subsurface layers is also difficult to model and dependent on the spatial resolution (e.g., Böning et al., 2016). For both, more observations are needed, including noble gas data to quantify the SMW and its circulation and dilution along the main spreading pathways. To validate coupled glacier-ocean models, tracers as He and Ne for SMW could be incorporated, and their modeled distributions compared with observations.

Our hydrographic and noble gas data illustrate the active glacier-ocean interaction in case of the 79NG. He and Ne observations provide robust results for SMW formation rates, independently from and compatible with other methods. In contrast to, e.g., moored instruments that examine temporal variability locally and allow investigating the forcing and response of submarine melting, noble gases are integrating tracers. Their observations allow us to quantify the formation and to elucidate the fate of SMW, its circulation and further mixing with ambient water masses.

Data Availability Statement

Noble gas (He, Ne) and transient tracer (CFC-11, CFC-12) data are public on the PANGAEA Data Publisher (https://doi.pangaea.de/10.1594/PANGAEA.931336). The CTD and bottle data are available on PANGAEA (CTD data: https://doi.org/10.1594/PANGAEA.871025, bottle data: https://doi.org/10.1594/PANGAEA.871028).

References

Aagaard, K., Swift, J. H., & Carmack, E. C. (1985). Thermohaline circulation in the Arctic Mediterranean Seas. *Journal of Geophysical Research*, *90*(C3), 4833. https://doi.org/10.1029/jc090ic03p04833

Beaird, N., Straneo, F., & Jenkins, W. (2015). Spreading of Greenland meltwaters in the ocean revealed by noble gases. *Geophysical Research Letters*, *42*(18), 7705–7713. https://doi.org/10.1002/2015GL065003

Beaird, N. L., Straneo, F., & Jenkins, W. (2018). Export of strongly diluted Greenland meltwater from a major glacial fjord. *Geophysical Research Letters*, *45*(9), 4163–4170. https://doi.org/10.1029/2018GL077000

Beckmann, J., Perrette, M., Beyer, S., Calov, R., Willeit, M., & Ganopolski, A. (2019). Modeling the response of Greenland outlet glaciers to global warming using a coupled flow line-plume model. The *Cryosphere*, *13*(9), 2281–2301. https://doi.org/10.5194/tc-13-2281-2019

Bieri, R., Koide, M., & Goldberg, E. D. (1964). Noble gases in sea water. *Science (New York, N.Y.)*, *146*(3647), 1035–1037. https://doi.org/10.1126/science.146.3647.1035

Böning, C. W., Behrens, E., Biastoch, A., Getzlaff, K., & Bamber, J. L. (2016). Emerging impact of Greenland meltwater on deepwater formation in the North Atlantic Ocean. *Nature Geoscience*, *9*(7), 523–527. https://doi.org/10.1038/ngeo2740

Bourke, R. H., Newton, J. L., Paquette, R. G., & Tunnicliffe, M. D. (1987). Circulation and water masses of the East Greenland shelf. *Journal of Geophysical Research*, *92*(C7), 6729–6740. https://doi.org/10.1029/JC092iC07p06729

Budéus, G., & Schneider, W. (1995). On the hydrography of the Northeast Water Polynya. *Journal of Geophysical Research 100*, pp. 4287–4299 C3. https://doi.org/10.1029/94JC02024

Bulsiewicz, K., Rose, H., Klatt, O., Putzka, A., & Roether, W. (1998). A capillary-column chromatographic system for efficient chlorofluorocarbon measurement in ocean waters. *Journal of Geophysical Research*, *103*(C8), 15959–15970. https://doi.org/10.1029/98JC00140

Choi, Y., Morlighem, M., Rignot, E., Mouginot, J., & Wood, M. (2017). Modeling the response of Nioghalvfjerdsfjorden and Zachariae Isstrøm glaciers, Greenland, to ocean forcing over the next century. *Geophysical Research Letters*, *44*(21), 071–111. https://doi.org/10.1002/2017GL075174

Craig, H., & Scarsi, P. (1997). Helium isotope stratigraphy in the GISP-2 ice core. *EOS Transactions AGU*, *78*(7).

Das, S. B., Joughin, I., Behn, M. D., Howat, I. M., King, M. A., Lizarralde, D., & Bhatia, M. P. (2008). Fracture propagation to the base of the Greenland ice sheet during supraglacial lake drainage. *Science*, *320*(5877), 778–781. https://doi.org/10.1126/science.1153360

Enderlin, E. M., Hamilton, G. S., Straneo, F., & Sutherland, D. A. (2016). Iceberg meltwater fluxes dominate the freshwater budget in Greenland's iceberg-congested glacial fjords. *Geophysical Research Letters*, *43*(21), 287–311. https://doi.org/10.1002/2016GL070718

Enderlin, E. M., Howat, I. M., Jeong, S., Noh, M. J., Van Angelen, J. H., & Van Den Broeke, M. R. (2014). An improved mass budget for the Greenland ice sheet. *Geophysical Research Letters*, *41*(3), 866–872. https://doi.org/10.1002/2013GL059010

Gade, H. G. (1979). Melting of ice in sea water: A primitive model with application to the Antarctic ice shelf and icebergs. *Journal of Physical Oceanography*, *9*(1), 189–198. https://doi.org/10.1175/1520-0485(1979)009%3C0189:MOIISW%3E2.0.CO;2

Grivault, N., Hu, X., & Myers, P. G. (2017). Evolution of Baffin bay water masses and transports in a numerical sensitivity experiment under enhanced Greenland melt. *Atmosphere-Ocean*, *55*(3), 169–194. https://doi.org/10.1080/07055900.2017.1333950

Hahm, D., Postlethwaite, C. F., Tamaki, K., & Kim, K.-R. (2004). Mechanisms controlling the distribution of helium and neon in the Arctic seas: The case of the Knipovich Ridge. *Earth and Planetary Science Letters*, *229*(1–2), 125–139. https://doi.org/10.1016/J.EPSL.2004.10.028

Hohmann, R., Schlosser, P., Jacobs, S., Ludin, A., & Weppernig, R. (2002). Excess helium and neon in the southeast Pacific: Tracers for glacial meltwater. *Journal of Geophysical Research*, *107*(C11), 3198. https://doi.org/10.1029/2000JC000378

Huhn, O., Hattermann, T., Davis, P. E. D., Dunker, E., Hellmer, H. H., Nicholls, K. W., et al. (2018). Basal melt and freezing rates from first noble gas samples beneath an ice shelf. *Geophysical Research Letters*, *45*, 8455–8461. https://doi.org/10.1029/2018GL079706

Huhn, O., Hellmer, H. H., Rhein, M., Rodehacke, C., Roether, W., Schodlok, M. P., & Schröder, M. (2008). Evidence of deep- and bottom-water formation in the western Weddell Sea. *Deep Sea Research Part II: Topical Studies in Oceanography*, *55*(8–9), 1098–1116. https://doi.org/10.1016/j.dsr2.2007.12.015

Jean-Baptiste, P., Petit, J., Lipenkov, V. Y., Raynaud, D., & Barkov, N. I. (2001). Constraints on hydrothermal processes and water exchange in Lake Vostok from helium isotopes. *Nature*, *411*(6836), 735–462. https://doi.org/10.1038/35078045

Jenkins, A. (1999). The impact of melting ice on ocean waters. *Journal of Physical Oceanography*, *29*(9), 2370–2381. https://doi.org/10.1175/1520-0485(1999)029%3C2370:TIOMIO%3E2.0.CO;2

Kjeldsen, K. K., Korsgaard, N. J., Bjørk, A. A., Khan, S. A., Box, J. E., Funder, S., et al. (2015). Spatial and temporal distribution of mass loss from the Greenland Ice Sheet since AD 1900. *Nature*, *528*(7582), 396–400. https://doi.org/10.1038/nature16183

Korhonen, M., Rudels, B., Marnela, M., Wisotzki, A., & Zhao, J. (2013). Time and space variability of freshwater content, heat content and seasonal ice melt in the Arctic Ocean from 1991 to 2011. *Ocean Science*, *9*(6), 1015–1055. https://doi.org/10.5194/os-9-1015-2013

Lindeman, M. R., Straneo, F., Wilson, N. J., Toole, J. M., Krishfield, R. A., Beaird, N. L., et al. (2020). Ocean circulation and variability beneath Nioghalvfjerdsbræ (79 north glacier) ice tongue. *Journal of Geophysical Research: Oceans*, *125*(8). https://doi.org/10.1029/2020JC016091

Loose, B., & Jenkins, W. J. (2014). The five stable noble gases are sensitive unambiguous tracers of glacial meltwater. *Geophysical Research Letters*, *41*(8), 2835–2841. https://doi.org/10.1002/2013GL058804

Mayer, C., Reeh, N., Jung-Rothenhäusler, F., Huybrechts, P., & Oerter, H. (2000). The subglacial cavity and implied dynamics under Nioghalvfjerdsfjorden Glacier, NE-Greenland. *Geophysical Research Letters*, *27*(15), 2289–2292. https://doi.org/10.1029/2000GL011514

Mayer, C., Schaffer, J., Hattermann, T., Floriciciu, D., Krieger, L., Dodd, P. A., et al. (2018). Large ice loss variability at Nioghalvfjerdsfjorden Glacier, Northeast-Greenland. *Nature Communications*, *9*(2768). https://doi.org/10.1038/s41467-018-05180-x

Mercenier, R., Lüthi, M. P., & Vieli, A. (2020). How oceanic melt controls tidewater glacier evolution. *Geophysical Research Letters*, *47*(8). https://doi.org/10.1029/2019GL086769

Minnett, P. J., Bignami, F., Böhm, E., Budéus, G., Galbraith, P. S., Gudmandsen, P., et al. (1997). A summary of the formation and seasonal progression of the Northeast Water Polynya. *Journal of Marine Systems*, *10*(1–4), 79–85. https://doi.org/10.1016/S0924-7963(96)00060-7

Mouginot, J., Rignot, E., Scheuchl, B., Fenty, I., Khazendar, A., Morlighem, M., et al. (2015). Fast retreat of Zachariæ Isstrøm, northeast Greenland. *Science*, *350*(6266), 1357–1361. https://doi.org/10.1126/science.aac7111

Oppenheimer, M., Glavovic, B. C., Hinkel, J., van de Wal, R., Magnan, A. K., Abd-Elgawad, A., et al. (2019). *Sea level rise and implications for low-lying islands, coasts and communities. IPCC special report on the ocean and cryosphere in a changing climate*. Retrieved from https://www.ipcc.ch/srocc/chapter/chapter-4-sea-level-rise-and-implications-for-low-lying-islands-coasts-and-communities/

Preußer, A., Heinemann, G., Willmes, S., & Paul, S. (2016). Circumpolar polynya regions and ice production in the Arctic: Results from MODIS thermal infrared with a regional focus on the Laptev Sea. *The Cryosphere*, *10*, 3021–3042. https://doi.org/10.5194/tc-10-3021-2016

Rhein, M., Steinfeldt, R., Huhn, O., Sültenfuß, J., & Breckenfelder, T. (2018). Greenland submarine melt water observed in the Labrador and Irminger sea. *Geophysical Research Letters*, *45*(19), 570–610. https://doi.org/10.1029/2018GL079110

Rignot, E., Fenty, I., Xu, Y., Cai, C., & Kemp, C. (2015). Undercutting of marine-terminating glaciers in West Greenland. *Geophysical Research Letters*, *42*(14), 5909–5917. https://doi.org/10.1002/2015GL064236

Rignot, E., & Kanagaratnam, P. (2006). Changes in the velocity structure of the Greenland Ice Sheet. *Science*, *311*(5763), 986–990. https://doi.org/10.1126/science.1121381

Schaffer, J. (2017). *Ocean impact on the 79 North Glacier, northeast Greenland*. Germany: University of Bremen. https://doi.org/urn:nbn:de:gbv:46-00106281-12

Schaffer, J., Kanzow, T., von Appen, W. J., von Albedyll, L., Arndt, J. E., & Roberts, D. H. (2020). Bathymetry constrains ocean heat supply to Greenland's largest glacier tongue. *Nature Geoscience*, *13*(3), 227–231. https://doi.org/10.1038/s41561-019-0529-x

Schaffer, J., von Appen, W. J., Dodd, P. A., Hofstede, C., Mayer, C., de Steur, L., & Kanzow, T. (2017). Warm water pathways toward Nioghalvfjerdsfjorden Glacier, Northeast Greenland. *Journal of Geophysical Research: Oceans*, *122*(5), 4004–4020. https://doi.org/10.1002/2016JC012462

Schlosser, P. (1986). Helium: A new tracer in Antarctic oceanography. *Nature*, *321*, 233–235. https://doi.org/10.1038/321233a0

Schneider, W., & Budéus, G. (1997). Summary of the Northeast Water Polynya formation and development (Greenland Sea). *Journal of Marine Systems*, *10*(1–4), 107–122. https://doi.org/10.1016/S0924-7963(96)00075-9

Sneed, W. A., & Hamilton, G. S. (2016). Recent changes in the Norske Oer Ice Barrier, coastal Northeast Greenland. *Annals of Glaciology*, *57*(73), 47–55. https://doi.org/10.1017/aog.2016.21

Straneo, F., Sutherland, D. A., Holland, D., Gladish, C., Hamilton, G. S., Johnson, H. L., et al. (2012). Characteristics of ocean waters reaching Greenland's glaciers. *Annals of Glaciology*, *53*(60). https://doi.org/10.3189/2012AoG60A059

Suess, H. E., & Wänke, H. (1963). On the possibility of a helium flux through the ocean floor. *Progress in Oceanography*, *3*, 347–353. https://doi.org/10.1016/0079-6611(65)90030-3

Sültenfuß, J., Roether, W., & Rhein, M. (2009). The Bremen mass spectrometric facility for the measurement of helium isotopes, neon, and tritium in water. *Isotopes in Environmental and Health Studies*, *45*(2), 83–95. https://doi.org/10.1080/10256010902871929

Syring, N., Lloyd, J. M., Stein, R., Fahl, K., Roberts, D. H., Callard, L., & O'Cofaigh, C. (2020). Holocene interactions between glacier retreat, sea-ice formation and Atlantic Water advection at the inner Northeast Greenland continental shelf. *Paleoceanography and Paleoclimatology*, *35*(11). https://doi.org/10.1029/2020pa004019

Van Den Broeke, M., Bamber, J., Ettema, J., Rignot, E., Schrama, E., Van Berg, W. J. D., et al. (2009). Partitioning recent Greenland mass loss. *Science*, *326*(5955), 984–986. https://doi.org/10.1126/science.1178176

Weiss, R. F. (1971). Solubility of helium and neon in water and seawater. *Journal of Chemical & Engineering Data*, *16*(2), 235–241. https://doi.org/10.1021/je60049a019

Well, R., & Roether, W. (2003). Neon distribution in South Atlantic and South Pacific waters. *Deep Sea Research Part I: Oceanographic Research Papers*, *50*(6), 721–735. https://doi.org/10.1016/S0967-0637(03)00058-X

Weppernig, R., Schlosser, P., Khatiwala, S., & Fairbanks, R. G. (1996). Isotope data from Ice Station Weddell: Implications for deep water formation in the Weddell Sea. *Journal of Geophysical Research*, *101*(C11), 25723–25739. https://doi.org/10.1029/96JC01895

Wilson, N., Straneo, F., & Heimbach, P. (2017). Satellite-derived submarine melt rates and mass balance (2011-2015) for Greenland's largest remaining ice tongues. The *Cryosphere*, *11*(6), 2773–2782. https://doi.org/10.5194/tc-11-2773-2017

Wilson, N. J., & Straneo, F. (2015). Water exchange between the continental shelf and the cavity beneath Nioghalvfjerdsbræ (79 North Glacier). *Geophysical Research Letters*, *42*(18), 7648–7654. https://doi.org/10.1002/2015GL064944

Yang, J., Luo, Z., & Tu, L. (2020). Ocean access to Zachariæ Isstrøm glacier, Northeast Greenland, revealed by OMG airborne gravity. *Journal of Geophysical Research: Solid Earth*, *125*(11). https://doi.org/10.1029/2020JB020281